PAPER • OPEN ACCESS

Controlling the gain contribution of background emitters in few-quantum-dot microlasers

To cite this article: F Gericke *et al* 2018 *New J. Phys.* **20** 023036

New Journal of Physics
The open access journal at the forefront of physics

Deutsche Physikalische Gesellschaft DPG
IOP Institute of Physics

Published in partnership with: Deutsche Physikalische Gesellschaft and the Institute of Physics

OPEN ACCESS

RECEIVED
13 September 2017

REVISED
11 December 2017

ACCEPTED FOR PUBLICATION
29 December 2017

PUBLISHED
15 February 2018

PAPER

Controlling the gain contribution of background emitters in few-quantum-dot microlasers

F Gericke[1], M Segnon[2], M von Helversen[1], C Hopfmann[1], T Heindel[1], C Schneider[3], S Höfling[3,4], M Kamp[3], A Musiał[1,5], X Porte[1], C Gies[2] and S Reitzenstein[1]

[1] Institut für Festkörperphysik, Technische Universität Berlin, D-10623, Berlin, Germany
[2] Institute for Theoretical Physics, University of Bremen, D-28334, Bremen, Germany
[3] Lehrstuhl für Technische Physik, Universität Würzburg, D-97074, Würzburg, Germany
[4] School of Physics and Astronomy, University of St Andrews, St Andrews, KY16 9SS, United Kingdom
[5] Present address: Laboratory for Optical Spectroscopy of Nanostructures, Department of Experimental Physics, Faculty of Fundamental Problems of Technology, Wrocław University of Science and Technology, Wrocław, Poland.

E-mail: stephan.reitzenstein@physik.tu-berlin.de

Keywords: nanolasers, cavity QED, high-β lasing, quantum dot–micropillar cavities, single quantum dot laser, semiconductor laser

Abstract

We provide experimental and theoretical insight into single-emitter lasing effects in a quantum dot (QD)-microlaser under controlled variation of background gain provided by off-resonant discrete gain centers. For that purpose, we apply an advanced two-color excitation concept where the background gain contribution of off-resonant QDs can be continuously tuned by precisely balancing the relative excitation power of two lasers emitting at different wavelengths. In this way, by selectively exciting a single resonant QD and off-resonant QDs, we identify distinct single-QD signatures in the lasing characteristics and distinguish between gain contributions of a single resonant emitter and a countable number of off-resonant background emitters to the optical output of the microlaser. Our work addresses the important question whether single-QD lasing is feasible in experimentally accessible systems and shows that, for the investigated microlaser, the single-QD gain needs to be supported by the background gain contribution of off-resonant QDs to reach the transition to lasing. Interestingly, while a single QD cannot drive the investigated micropillar into lasing, its relative contribution to the emission can be as high as 70% and it dominates the statistics of emitted photons in the intermediate excitation regime below threshold.

1. Introduction

On the way towards the ultimate thresholdless semiconductor nanolaser [1], with only a single quantum dot (QD) as gain medium, the three main challenges are (i) developing the required technology to realize such devices, (ii) identifying lasing threshold, and (iii) proving experimentally that a single QD is solely responsible for reaching it. Recent advances in material quality and the fabrication of semiconductor micro- and nano-lasers have already allowed researchers to approach the regime where a single QD can substantially modulate the optical gain [2–7]. So far, self-assembled QDs in semiconductor microcavities feature the highest optical quality in terms of oscillator strength, quantum efficiency and coherence properties [8], giving a chance to eventually approach the single-emitter lasing regime. However, in the presently available QD-cavity systems non-negligible gain contribution by non-resonant transitions is still necessary to overcome the laser threshold [5, 9, 10]. To better control the coupling behavior and the gain contribution of a single resonant emitter, integrating a single self-assembled QD into a high-quality microcavity will be interesting in further optimizations. However, this integration is a complicated task that requires sophisticated techniques, such as site-controlled growth [11–15] or *in situ* lithography [16–18]. Deterministically-positioned QDs have been successfully applied in the past to realize high-quality single-photon sources [19, 20], but up until now have not been demonstrated to provide sufficient optical gain to reach the lasing threshold in a single-QD device.

In contrast, state-of-the-art QD-based microlasers have solely been based on self-assembled QDs placed randomly on the active area of the microlaser [2, 3, 5]. Most of these QDs can contribute to the output of the microlaser in an uncontrolled way, and only a small fraction of them have suitable spectral positions so they can be tuned through the cavity mode by, e.g., temperature tuning. Eventually, scenarios with only a single QD in spectral resonance (but not necessarily spatially matched) with the cavity mode are possible. Nevertheless, the requirements for such a single QD device to lase are very demanding. Even for a spontaneous emission factor (β-factor) close to unity, in which case spontaneous emission of the resonant emitter is almost solely directed into the laser mode, the light–matter coupling rate has to overcome the cavity loss rate at least by a factor of two [21]. In practice, it requires to combine cavities with a high quality factor (Q) and strong light–matter interaction, leading towards the coherent strong coupling regime [10, 22]. In this case the required high Q-factor microresonators with small mode volumes foster the illumination of the cavity mode by off-resonant QDs [23, 24] which in turn has significant impact on the transition to lasing. Here, even spectrally far off-resonant emitters can couple to the cavity mode by a combination of different mechanisms, i.e., due to the interaction of QD excitations with acoustic phonons [25], Auger-like scattering processes [26, 27, 34] and Coulomb interaction with multi-exciton states [28]. By these mechanisms, off-resonant QDs can feed the cavity mode within a wide energy range of tens of meV and contribute to lasing. In the regime of increased excitation that is typical for laser applications, the dominant mechanism is the formation of multi-exciton states, the transitions of which can be in close spectral vicinity to the cavity mode even if the associated exciton resonance is strongly detuned. Small remaining energy differences on the meV scale are efficiently bridged predominantly by Auger-assisted scattering of carriers in the QD states with carriers in WL states that are occupied at sufficiently strong excitation at which QD emission saturates. This combination has been demonstrated to form an emission background that is resonant with the mode [26, 28, 43]. In this context, a better understanding of the influence of individual in- and off-resonant QDs on the lasing behavior is needed and will be crucial for the design and operation of future micro- and nano-lasers. This information is also an important contribution to the ongoing very active discussion in the semiconductor community about the possibility for a single QD to provide enough gain to initiate and sustain lasing [10, 29–33]. Interestingly, and in spite of their central role, the influence of off-resonantly coupled QDs on the lasing behavior has not been described in a controlled and comprehensive way so far. We address this open issue by using a versatile two-color excitation scheme with support from a microscopic laser theory. Our research gives important insight on the impact of background gain provided by off-resonant QDs in a regime where the emission is dominated by a single resonant QD.

The structure under study is a high-quality low-mode volume GaAs-based QD-micropillar cavity containing a single layer of self-assembled QDs with an inhomogeneously broadened energy distribution of $\approx$50 meV. Our goal is to control the gain contribution of off-resonantly coupled QDs in our microlaser and to distinguish their influence on the lasing behavior from that of the desired resonant QD. This allows us to identify fingerprints of different gain contributions to the laser output and, as a result, distinguish between devices with only one QD and with a few QDs constituting the gain of the microlaser, simply by varying the relative intensity of two excitation lasers. We do so by using a two-color excitation scheme: the target QD gain is selectively addressed by resonant excitation of its spectrally narrow p-shell resonance, while the gain of the off-resonantly coupled QDs is controlled simultaneously by above-band excitation. Thereby, the ratio between the two different excitation powers is used to control the relative contribution of the off-resonant emitters to the device output. A similar excitation approach has been used previously to control the gain in optical amplifiers from additional quantum-dashes in addition to a quantum-well gain, enabling a novel mechanism for lasing based on a two-photon excitation process [55]. In general, nanolasers operating in the high-β regime do not show a pronounced and typical laser characteristics in the input–output curve [32]. Therefore, the identification of the lasing threshold for a nanolaser is a challenging task that usually requires to take into account different emission characteristics including the photon statistics of emission [7, 35–41]. In this context, we apply a microscopic semiconductor laser model to precisely determine the threshold of the investigated microlaser in the different experimental scenarios. Following this approach, we obtain a comprehensive understanding of the laser's threshold and its β-factor, which in our experiment is a function of the background gain contribution due to the different coupling coefficients of the resonant QD and background (BG) emitters.

2. Materials and methods

2.1. Sample properties

For our present study it is crucial that the QD in resonance couples efficiently to the cavity mode and that the contribution of the off-resonant emitters to the laser output is non-negligible. Therefore, we have used a high quality factor ($Q \approx 15000$) low-mode volume micropillar with a diameter of 1.8 μm, maximizing the light–matter coupling strength between the exciton transition of the resonant QD and the fundamental cavity mode.

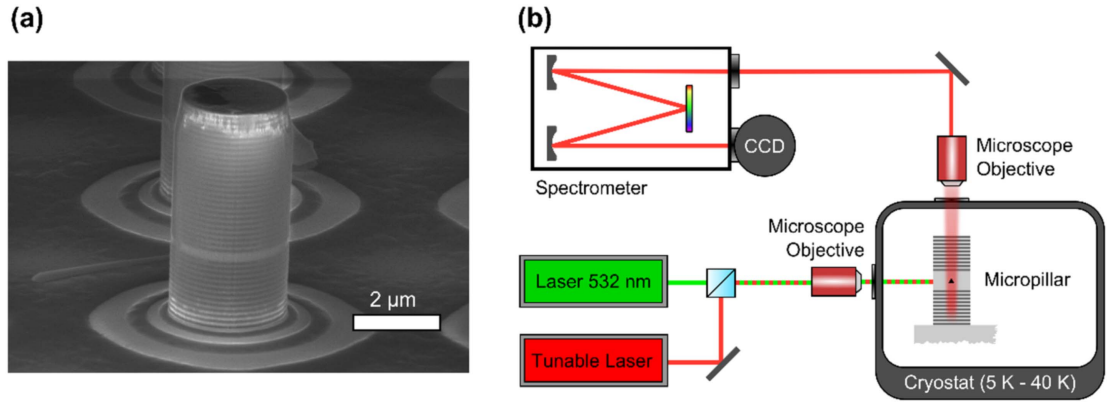

Figure 1. (a) Scanning electron micrograph (SEM) of an exemplary processed free standing micropillar. The bottom distributed Bragg reflector (DBR) is only partly etched. (b) Sketch of the experimental micro-photoluminescence (μPL) setup with a configuration of lateral excitation and axial detection.

The gain medium consists of a single layer of self-assembled InGaAs QDs, with an Indium content of about 40% and an areal density of 10^{10} cm^{-2} in the center of a GaAs λ-cavity. These QDs feature a large oscillator strength, which in combination with the low mode-volume micropillar ensures pronounced light–matter interaction that facilitates reaching the strong coupling regime [24] with pronounced single QD lasing effects [10]. On top (bottom) of the central GaAs cavity 26 (30) pairs of AlAs/GaAs layers acting as high reflective distributed Bragg reflectors (DBR) were grown. The micropillar was realized by high-resolution electron-beam lithography and plasma etching. A scanning electron micrograph of a processed free standing micropillar is shown in figure 1(a). The λ-cavity is visible in this picture as the thicker central horizontal section. The sample was cleaved to gain optical access to the micropillar cavity from the side (in the direction perpendicular to the micropillar axis). This enables direct and wavelength-independent excitation of the QDs [44]. For further details on the sample layout and processing we refer to [45].

To gain insight into the lasing characteristics of the QD-micropillar structure, its optical output was studied as a function of excitation power using the micro-photoluminescence (μPL) setup schematically shown in figure 1(b). This setup has a perpendicular configuration of the excitation and the detection paths. The main advantage of side-excitation here is that the laser light is not (partially) blocked by the stop-band of the top DBR [46]. Therefore, an efficient and homogeneous, i.e. wavelength-independent, excitation of the QDs can be realized. Furthermore, the perpendicular excitation and detection paths provide a natural rejection of a large fraction of the pump lasers' light in detection—an advantage that is particularly important for pumping wavelengths close to the micropillar's resonance frequency. To selectively excite a single QD resonant with the cavity mode, we apply a quasi-resonant p-shell excitation scheme using a tunable semiconductor infrared (IR) laser with linewidth below 100 kHz (0.41 neV). The optical above-band excitation of the sample is carried out by a frequency doubled Nd:YAG laser emitting at a wavelength of 532 nm (further referred to as green excitation). The output power of each laser can be independently attenuated via a set of variable density filters before they are combined on a beam-splitter and focused on the sample by a lateral objective featuring high numerical aperture of 0.4 and long working distance of 20 mm. The sample is mounted in a variable temperature He-flow cryostat and kept at constant temperature of 25 K for most of the experiments. The far-field emission of the fundamental cavity mode is in perpendicular direction to the excitation path.

Based on the areal QD density of the wafer, we estimate an amount of $\cong$250 dots within the active layer of a micropillar with 1.8 μm diameter. Due to the self-assembled character of QD growth, there is a high variability in the QD emission energy and the spatial position. Nevertheless, about 5 QD lines are in the spectral proximity of the lasing mode and can be studied by fine-tuning with respect to the cavity mode. In the present case, the chosen QD excitonic transition couples strongly to the cavity mode at a resonance temperature of 25 K. At the same time, the spectral density of spectator QDs is high enough to provide enough background gain to overcome the lasing threshold.

Above-band excitation is used to excite the BG emitters. Carriers are generated in the barrier material, from where they are captured equally into all QDs irrespective of their transition energies. In contrast, to address a target QD selectively either a resonant (s-shell) or a quasi resonant (p-shell) excitation scheme has to be employed. We choose p-shell excitation for most of the experiments because, in comparison with s-shell excitation, laser stray-light suppression is less demanding and to rule out a possible transfer of coherence from the exciting laser to the microlaser. To determine the energy of the p-shell for QDs in the micropillar of interest, we perform an excitation wavelength-dependent measurement, i.e. micro-photoluminescence excitation

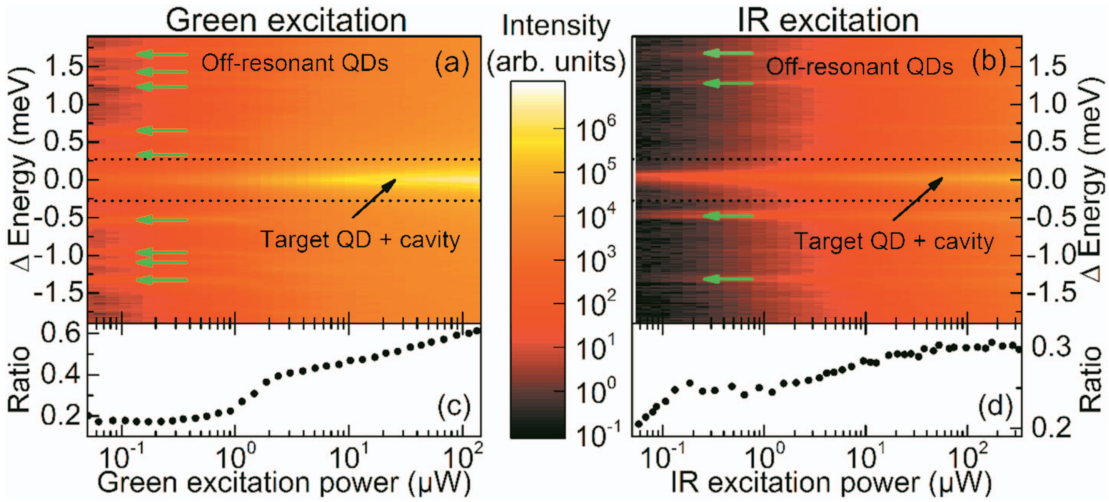

Figure 2. Power-dependent emission spectra for the case of only above-band (green) excitation (a) and only p-shell (IR) excitation of the target QD in resonance with the cavity mode (b). The energy difference is relative to the central energy of the cavity mode emission at high excitation powers. The off-resonant QDs are marked by green arrows. Panels (c) and (d) show the ratio of the integrated total single QD and cavity mode intensity (area between the black dotted lines in (a) and (b)) and the residual area of the spectrum for the two respective excitation schemes.

(μPLE), at low excitation powers (not shown here). Whenever the laser energy is resonant with a p-shell (or another higher energy resonance) of a QD, we see a sharp maximum in the emission intensity at the energy of this QD and the cavity mode due to efficient pumping of the corresponding QD followed by the excitation transfer into the cavity mode due to off-resonant QD-cavity coupling. The response of the mode gets stronger the less detuned a QD is with respect to the cavity due to more efficient non-resonant cavity feeding. We selected the QD with the strongest p-shell resonance to coherently interact with the cavity mode. It can be tuned into resonance with the laser mode and exhibits a splitting between the s-shell and the p-shell of $\approx$13 meV. This splitting is small in comparison to typical values of $\sim$25–30 meV for standard In(Ga)As QDs [47–49], which is in agreement with an enhanced in-plane spatial extension of investigated QDs with enhanced oscillator strengh of about 25.

2.2. Optical characterization

First, we evaluate the influence of the BG emitters on the microlaser characteristics by examining the power-dependent emission spectra in two limiting cases: selective p-shell excitation of a target QD in resonance with the cavity mode (figure 2(a)) and non-selective above-band excitation with a green laser of all QDs in the gain medium (figure 2(b)).

The qualitative differences between the two cases are visible in the two panels of figure 2. Using above-band excitation (figure 2(a)), the QD emission lines (indicated by green arrows) exhibit larger linewidths at low excitation and broaden strongly with increasing excitation power. At high excitation $\geqslant$5 μW, the spectrum is dominated by the cavity mode and strong broadband background so that single QD emission lines cannot be resolved anymore. These observations can be attributed to the fact that a large number of high-energy carriers are created in the whole structure that undergo multi-stage relaxation processes into the lowest energy states in the QDs. At higher excitation powers, when the confined states in the QDs are saturated, the recombination takes place from higher-energy states in the structure (wetting layer, WL or GaAs barrier material). This constitutes an additional background that contributes to the output of the micropillar, and it eventually gets stronger than the emission from single QDs experiencing saturation. In contrast, figure 2(b) depicts the spectral dependence when only the p-shell of the selected QD is pumped. Due to a lower amount of carriers and less decoherence in the system, QD lines are narrower and do not broaden significantly with increasing excitation power, so that they can be individually resolved in the whole covered excitation range. Interestingly, even though we are using quasi-resonant excitation of a target QD, off-resonant QDs are still visible in the spectrum. This observation can be explained by the strong light–matter coupling in the structure leading to cavity mediated coupling between the QDs as discussed above. In this process, a target QD emits a photon that is stored in the cavity and afterwards transferred via one of the off-resonant coupling mechanisms, i.e. interaction with acoustic phonons, Auger-like scattering or Coulomb interaction with multi-excitonic states, to an off-resonant QD. An analog effect was previously observed in resonance fluorescence (RF) experiments on the same sample [50]. Another possibility is that due to relatively shallow confining potential of the investigated QDs, the p-shell

overlaps energetically with the tail of the density of states in the WL. This would result in non-zero probability of scattering carriers created in the p-shell state out of the QD towards the WL [51] (instead of relaxing to the s-shell of the target QD). Since carriers in the WL can be captured into any of the QDs in the active region, this effect would be a detrimental factor to the selectiveness of our quasi-resonant excitation scheme.

To further quantify the difference in the response of the system under the two applied excitation schemes, we evaluate the single QD and the BG emitters' contribution to the spectra in terms of integrated intensities. For this purpose, we calculate the ratio between the QD in resonance with the cavity mode (selected range is marked as dotted lines in figures 2(a) and (b)) and the integrated intensity of the rest of the presented spectrum (outside the dotted lines). Figure 2(c) depicts the system response under non-resonant excitation. The ratio shows a strong nonlinear increase in favor of the cavity mode contribution starting from $P \approx 1\ \mu$W showing that most of the emission is funneled into the cavity mode and contributes to the microlaser output. This can be attributed to reaching the onset of stimulated emission and resembles a typical input–output laser characteristics. With increasing excitation power, the cavity is more effectively fed by the off-resonant emitters, which is reflected in a decreasing contribution of their intensity to the total intensity—a behavior that we consider as fingerprint of lasing action. Figure 2(d) shows the described ratio for the quasi-resonant IR pumping scenario. Noteworthy, at low excitation powers, under p-shell excitation the cavity is fed more efficiently than when the above-band pump is applied, as it is indicated by the ≈7% higher value of the ratio at low pump powers. This behavior can be attributed to strong coupling of the single QD in resonance to the cavity mode. The steeper initial increase in the ratio of the intensities is a fingerprint of the single-QD nonlinearity proving that indeed in this excitation range the contribution of the BG emitters is negligible. The subsequent power-dependent evolution differs strongly from the above-band excitation scenario depicted in figure 2(c). For the p-shell excitation of the target QD, the ratio stays almost constant within ≈5%–10% variation and does not scale proportionally to the excitation power. This supports the interpretation that excitation of the system comes almost exclusively from a single emitter (at low excitation powers), which undergoes saturation for intermediate to high excitation powers.

2.3. Microscopic laser model for resonant QD and BG emitters

To gain further insight in the presented input–output curves and their interrelation with single-QD lasing, we employ a theoretical laser model that accounts for the semiconductor gain medium. As discussed in the introduction, a combination of non-resonant coupling mechanisms causes detuned transitions to emit *resonantly* into the cavity mode. For this reason, we use an effective picture, where the resonant contributions of N_{BG} BG emitters are accounted for along the lines of Re. 43, and their Jaynes–Cummings coupling with the cavity mode is considered in addition to the gain of the main single, resonant QD. In the following, we label quantities referring to the single QD with $\xi = \mathrm{QD}$ and those referring to transitions of the BG emitters with $\xi = \mathrm{BG}$. Our microscopic model is based on the approach introduced in [52] and consists of a set of coupled dynamical equations derived from the Hamiltonian for the electronic states of the QD emitters, photons of the quantized electromagnetic field, and the interaction between QD excitations and photons in the laser mode. A set of coupled dynamical equations is derived for the intracavity mean photon number ($\langle b^\dagger b\rangle$), and carrier populations in the resonant QD ($f^{e,h}_{s,\mathrm{QD}}$) and the off-resonant QD transitions ($f^{e,h}_{s,\mathrm{BG}}$):

$$\left(\hbar\frac{\mathrm{d}}{\mathrm{d}t} + 2\kappa\right)\langle b^\dagger b\rangle = 2\,|g_{\mathrm{QD}}|^2\,\langle b^\dagger v^\dagger c\rangle_{\mathrm{QD}} + 2N_{\mathrm{BG}}\,|g_{\mathrm{BG}}|^2\,\langle b^\dagger v^\dagger c\rangle_{\mathrm{BG}} \tag{1}$$

$$\hbar\frac{\mathrm{d}}{\mathrm{d}t}f^{e,h}_{s,\mathrm{QD}} = -2\,|g_{\mathrm{QD}}|^2\,\langle b^\dagger v^\dagger c\rangle_{\mathrm{QD}} + R_{\mathrm{nl}}(\beta_{\mathrm{QD}}) + R^{e,h}_{p\to s}(P_{\mathrm{g}}, P_{\mathrm{IR}}), \tag{2}$$

$$\hbar\frac{\mathrm{d}}{\mathrm{d}t}f^{e,h}_{s,\mathrm{BG}} = -2\,|g_{\mathrm{BG}}|^2\,\langle b^\dagger v^\dagger c\rangle_{\mathrm{BG}} + R_{\mathrm{nl}}(\beta_{\mathrm{BG}}) + R^{e,h}_{p\to s}(P_{\mathrm{g}}, P_{\mathrm{IR}}), \tag{3}$$

Here κ is the cavity loss rate, g_ξ denotes the coupling constant of the QD in resonance or that of the off-resonant emitters, and the operators $c^\dagger$, $v^\dagger$ annihilate (create) a carrier in the s-shell conduction- or valence-band state of each emitter. Operators $b^\dagger$ address photons in the laser mode. The rate $R^{e,h}_{p\to s}$ describes the creation of excited carriers in the laser levels via scattering that follows excitation from the two pump sources, green and IR, with respective pump powers P_{g} and P_{IR}. These excited carriers are created into the energetically higher p-states via a relaxation-time approximation. The spontaneous recombination of carriers into nonlasing modes is given by the rate R_{nl} that depend on the β-factors of the resonant QD (β_{QD}) and the BG emitters (β_{BG}). The dynamics of equations (1)–(3) is determined by a balance of these interaction processes with the environment and the light–matter interaction of the single resonant and N_{BG} background QDs via photon-assisted polarizations

$$\left(\hbar\frac{\mathrm{d}}{\mathrm{d}t} + \kappa + \Gamma_\xi\right)\langle b^\dagger v^\dagger c\rangle_\xi = f^e_{s,\xi} f^h_{s,\xi} + (1 - f^e_{s,\xi} - f^h_{s,\xi})\,\langle b^\dagger b\rangle \tag{4}$$

with the dephasing Γ_ξ associated with the QD transitions resonant with the laser mode. This equation contains the spontaneous-emission contribution $\propto f^e f^h$ and the stimulated emission or absorption terms proportional to

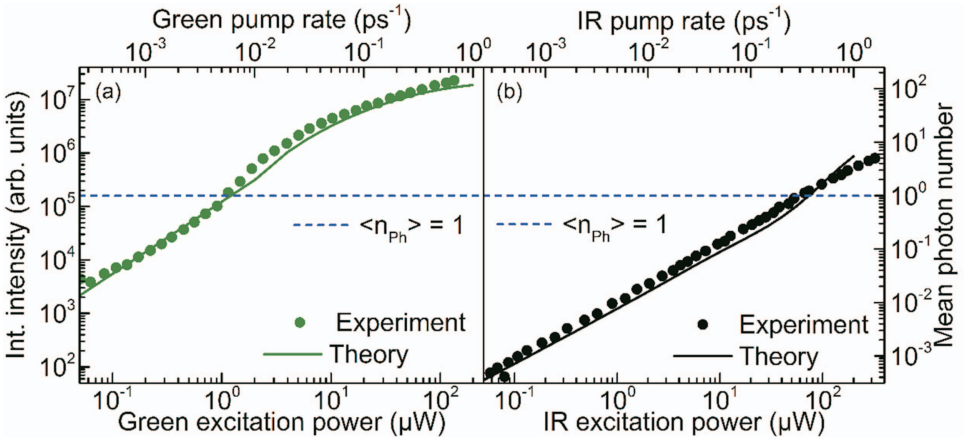

Figure 3. Experimental (dots) and theoretical (line) input–output characteristics for (a) only exciting above-band (green) and (b) only exciting the p-shell of the target QD (IR). The experimental points of the target QD in resonance with the cavity mode were calculated by integrating the Rabi-doublet area of the spectra, delimited with dotted lines in figures 2(a) and (b). In both panels the laser threshold, defined in the numerical model as $\langle n_{\mathrm{Ph}} \rangle = 1$, is indicated with a dashed blue line.

the intra-cavity mean photon number that also appears in rate–equation theories. While the rate equations could be obtained by adiabatically eliminating the photon-assisted polarizations, we calculate the full dynamics and the dynamics of higher-order carrier-photon correlations $\delta\langle b^\dagger bc^\dagger c\rangle$, $\delta\langle b^\dagger bv^\dagger v\rangle$, $\delta\langle b^\dagger b^\dagger bv^\dagger c\rangle$, and $\delta\langle b^\dagger b^\dagger bb\rangle$ as described in the appendix B. These equations allow us to calculate the second-order photon-correlation function at zero time delay $g^{(2)}(\tau = 0)$, which contains information on the statistical properties of the emission differentiating between single-photon character ($g^{(2)}(\tau = 0) < 1$), thermal ($g^{(2)}(\tau = 0) = 2$), and coherent ($g^{(2)}(\tau = 0) = 1$) emission.

We determine the light–matter coupling-strength g_ξ and the β-factor individually for the resonant and off-resonant case on the basis of experimental data obtained under purely green or IR excitation as shown in figure 3, see appendix B for further details. These parameters are used in all the following calculations and only the pump rates are varied to obtain the two-color excitation plots.

To further understand the nature of excitation in our system, it is important to note that the two components of the gain in our laser model (resonant QD and BG emitters) are coupled via the common light field of the cavity. This leads to the effect that the resonant QD can in fact be indirectly excited by background excitation by reabsorbing cavity photons that were emitted from the detuned BG emitters, and vice-versa. It is therefore not possible to separate the system into resonant and background parts other than by switching off the corresponding light–matter coupling completely, a possibility that is reserved to theory alone and that has been used to obtain figure 6(c).

Our evaluation of the experimental data using non-resonant excitation confirms that emitters that are spectrally and spatially detuned from the cavity mode exhibit a weaker light–matter coupling strength and, thus, a lower β-factor than the single QD in resonance with the cavity mode. Consequently, the β-factor of the coupled system consisting of resonant and BG emitters depends sensitively on the contribution of each of them. It is possible to quantify an effective β-factor from equations (2) to (4) by considering only the spontaneous-emission contributions and solving equation (4) adiabatically. In this case, an effective β-factor can be expressed as (see appendix B)

$$\beta_{\mathrm{eff}} = \frac{\beta_{\mathrm{QD}}}{1 + \frac{N}{\lambda}\frac{\langle b^\dagger v^\dagger c\rangle_{\mathrm{BG}}}{\langle b^\dagger v^\dagger c\rangle_{\mathrm{QD}}}} + \frac{\beta_{\mathrm{BG}}}{1 + \frac{\lambda}{N}\frac{\langle b^\dagger v^\dagger c\rangle_{\mathrm{QD}}}{\langle b^\dagger v^\dagger c\rangle_{\mathrm{BG}}}}, \qquad \lambda = \frac{\beta_{\mathrm{BG}}}{\beta_{\mathrm{QD}}}\left|\frac{g_{\mathrm{QD}}}{g_{\mathrm{BG}}}\right|^2. \tag{5}$$

In the limit of vanishing contributions from BG emitters, β_{eff} takes on the high β_{QD} value of the resonant emitter, whereas a significantly lower $\beta_{\mathrm{eff}} = \beta_{\mathrm{BG}}$ is observed in the case of a dominating background. Via λ, not only the number of BG emitters enters, but also the respective coupling strength, taking into account the weaker coupling of detuned emitters.

The value of this effective β-factor β_{eff} implicitly depends on the excitation rates of resonant and BG emitters and can, thereby, be tuned as we discuss in the following section. Note that more intricate many-body effects can already lead to deviations from a constant β-factor of the resonant and BG QDs (β_{BG} and β_{QD}), a more detailed study of which is beyond the scope of the present work [42, 43].

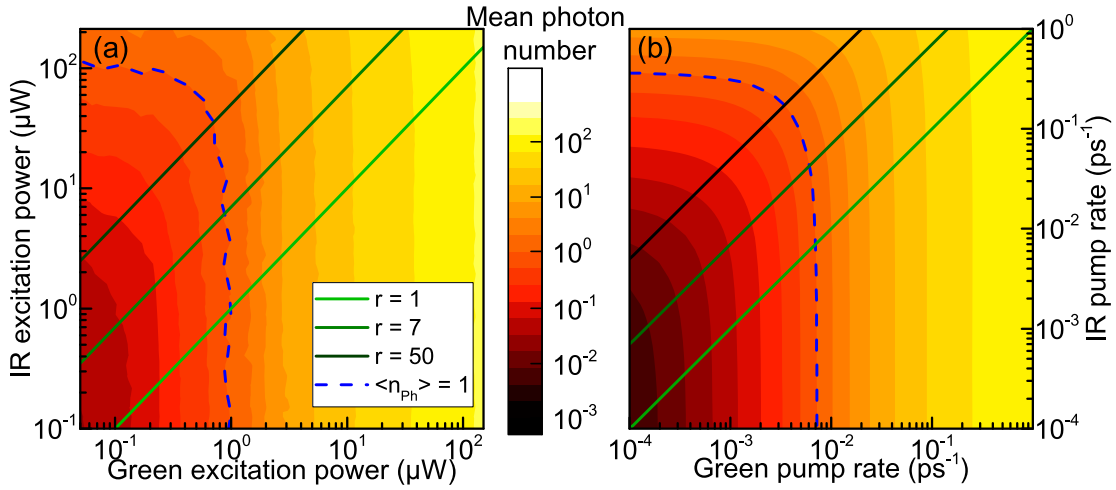

Figure 4. Experimental (left) and modeled (right) dependence of the emission intensity on the excitation conditions in the two-color excitation scheme. The blue dashed line in both panels represents the lasing threshold according to the usual definition $\langle n_{\mathrm{Ph}} \rangle = 1$ for microlasers. Above this line (lighter colors areas) the micropillar output is dominated by stimulated emission. The ratio r is defined as the excitation power of the green laser divided by the excitation power of the IR laser.

3. Results and discussion

3.1. Background controlled lasing in a QD-micropillar system

The experimental input–output curves for the two limiting cases, using only above-band excitation and only quasi-resonant p-shell excitation of the target QD are shown in figures 3(a) and (b) together with the theoretical results. The latter ones are plotted versus the respective pump rates, which we consider to depend linearly with the excitation powers. The Appendix A provides details on how the input-parameters for the theory are determined from the results presented in figure 3. In the case of above-band excitation, in which all QDs are excited and can contribute to the gain, the input–output dependence shows the pronounced s-shape that is characteristic for the onset of stimulated emission in microlasers. In contrast, the p-shell excitation scenario results in nearly linear behavior over the whole measured range. Noteworthy, saturation at some point on the input–output curve would be expected for this latter scenario, but is not observed. Further experiments (see appendix) in a resonant pumping scenario demonstrate that the QD in resonance is indeed saturating under strong p-shell excitation. However, the fact that we do not observe saturation in the input–output curve (see figure 3(b)) shows that the off-resonant emitters are also (unintentionally) excited and can even dominate the output of the QD-micropillar at high pump rates.

The clearly different behavior between both panels in figure 3 demonstrates that our two-color excitation scheme can be used to both understand and tailor the output characteristics of a few-QD semiconductor microlaser, including the β-factor, by selective manipulation of the resonant and background gain contribution.

Up to now, the two limiting cases of either exciting dominantly the single target QD or all QDs in the micropillar have been presented. Now, we analyze the transition between them by gradually unbalancing between the two different pumps and continuous measurement of the QD-micropillar output characteristics. The results of full two-color excitation measurements are shown as excitation maps in figure 4 as obtained from experiment (panel (a)) and from the theoretical model (panel (b)).

The horizontal axis represents the strength of the above-band excitation. Increasing the corresponding pump-rate corresponds mainly to increased excitation of the off-resonant emitters in the micropillar. In the vertical direction, p-shell excitation of the target single QD is increased. The blue dashed line in the left panel corresponds to the usual definition of threshold power ($\langle n_{\mathrm{Ph}} \rangle = 1$), determined from the numerical calculations by matching the calculated input–output characteristics to the experimentally measured one. Noteworthy, the qualitative agreement between the experimental and the theory maps is very high. The presented maps prove that the difference between input–output curves for the limiting cases is not related to different scaling factors for the excitation power but indeed to the fact that achieving lasing conditions with a single QD gain is rather challenging.

To visualize the change in the shape of the input–output curve, diagonal cross-sections through the 2D map are presented in figure 5 at positions indicated by the colored solid lines in figure 4(a). The upper- and lower-most input–output curves correspond to the two limiting cases shown in figures 3(a) and (b). The diagonal cross-sections correspond to the input–output characteristics at fixed ratios $r = 1, 7, 50$ between both excitation

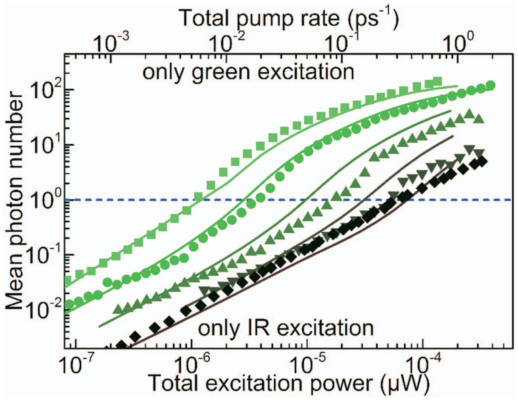

Figure 5. Diagonal cross-sections through the 2D map (indicated with the corresponding colors in the previous figure) for three different green to IR excitation power ratios $r = 1, 7$ and 50 (corresponding to constant relative contribution of the off-resonant emitters to the gain) together with the previously shown limiting cases are plotted versus the sum of both excitation powers. The symbols correspond to the experimental data of the 2D map and the lines to the calculations shown in figure 4. The blue dashed line indicates the lasing threshold ($\langle n_{\mathrm{Ph}} \rangle = 1$) as extracted from the theory fit to the experimental data.

powers, i.e., constant contribution-percentage of the off-resonant emitters. The input–output curves in figure 5 are plotted against the sum of both excitation powers. The complementary theory curves are also shown in the same panel together with a horizontal (blue dashed) line associated with a mean photon number $\langle n_{\mathrm{Ph}} \rangle = 1$, indicative for the lasing threshold. It can be clearly seen that the increase of the off-resonant emitter-contribution causes the s-shape in the transition regime to become more pronounced and the threshold position shifts towards lower total excitation powers. Interestingly, the higher fraction of light coupled into the cavity mode from the BG emitters with less ideal light–matter coupling strength simultaneously degrades the effective β-factor of the emission. We quantify this effect on the basis of equation (5), which is evaluated numerically. The result is shown in figure 6(a): the maximal achievable effective β-factor of 0.37 in case of dominant p-resonant excitation is still more than two times smaller than the β-factor for the target resonant QD, which we extract to be 0.9 from matching the result shown in figure 3 for selective IR excitation of the single QD only (without any background emission). This indicates that even weak above-band excitation with a pump rate as low as 10^{-4} ps^{-1} introduces significant BG-emitter related occupation of the cavity mode. Noteworthy, for only above-band excitation of the system and in the strong excitation regime, the effective β-factor drops to values close to $\beta_{\mathrm{BG}} = 0.25$, evidencing the dominant role of the BG emitters in this range. Only in the regime of intermediate IR pump rates, the single QD gains a meaningful contribution so that its fingerprint becomes visible in the microlaser characteristics. In this low excitation regime, these characteristics distinguish between a microlaser with only single-QD gain and a multi-QD laser.

Similar regions can be identified in the photon statistics. The calculated $g^{(2)}(\tau = 0)$ map is presented in figure 6(b). Also in this case the behavior is non-monotonic with P_{IR}: generally, in the low excitation regime, $g^{(2)}(\tau = 0) = 2$ reflects the thermal character of the emission from the QD ensemble. This at first sight unexpected behavior is explained by the fact that a small fraction of P_{IR} also drives the background. In a realistic case of exciting 100 BG emitters by 1%, their spontaneous emission becomes comparable to the contribution of the single resonant QD. Then light is thermal, because the single-QD becomes 'part of the ensemble'. With increasing carrier population, i.e. high P_{IR} spontaneous emission becomes faster, as it is proportional to the populations ($f_e \times f_h$), and once inversion is reached, stimulated emission sets in for the single-QD but not for the BG emitters. Therefore, the single-QD contribution dominates the statistical properties of the emission only at higher excitation, revealing non-classical behavior and antibunching. Interestingly, even if there was no fraction of P_{IR} driving the background, we would observe a similar effect, because photons emitted into the cavity by the single-QD were re-absorbed by the background QDs, so that even then, the emission would be thermal at very low P_{IR}. At high incoherent excitation (using P_{G}) coherent emission is reached at pump rates of about 0.1 ps^{-1}. Since a small fraction of the p-shell excitation also drives the BG emitters, coherent emission can also be approached when P_{IR} is further increased, even though the single-QD alone does not provide sufficient gain to cross the laser threshold. Noteworthy, from $g^{(2)}(\tau = 0) > 1$ (see figure 6(b)) we can conclude that the laser emission is not reached for the maximum P_{IR} values used in our experiment (despite of $\langle n_{\mathrm{Ph}} \rangle \geqslant 1$).

Both the effective β-factor and $g^{(2)}(\tau = 0)$ dependences on the excitation power can be traced back to the relative contribution of the single-QD and BG emitters to the output of the microlaser presented in figure 6(c). This intensity map presents the relative contribution of a single QD to the emission evaluated as a relative difference between the total emission (BG emitters and the single-QD) and the BG emitters' emission only (in

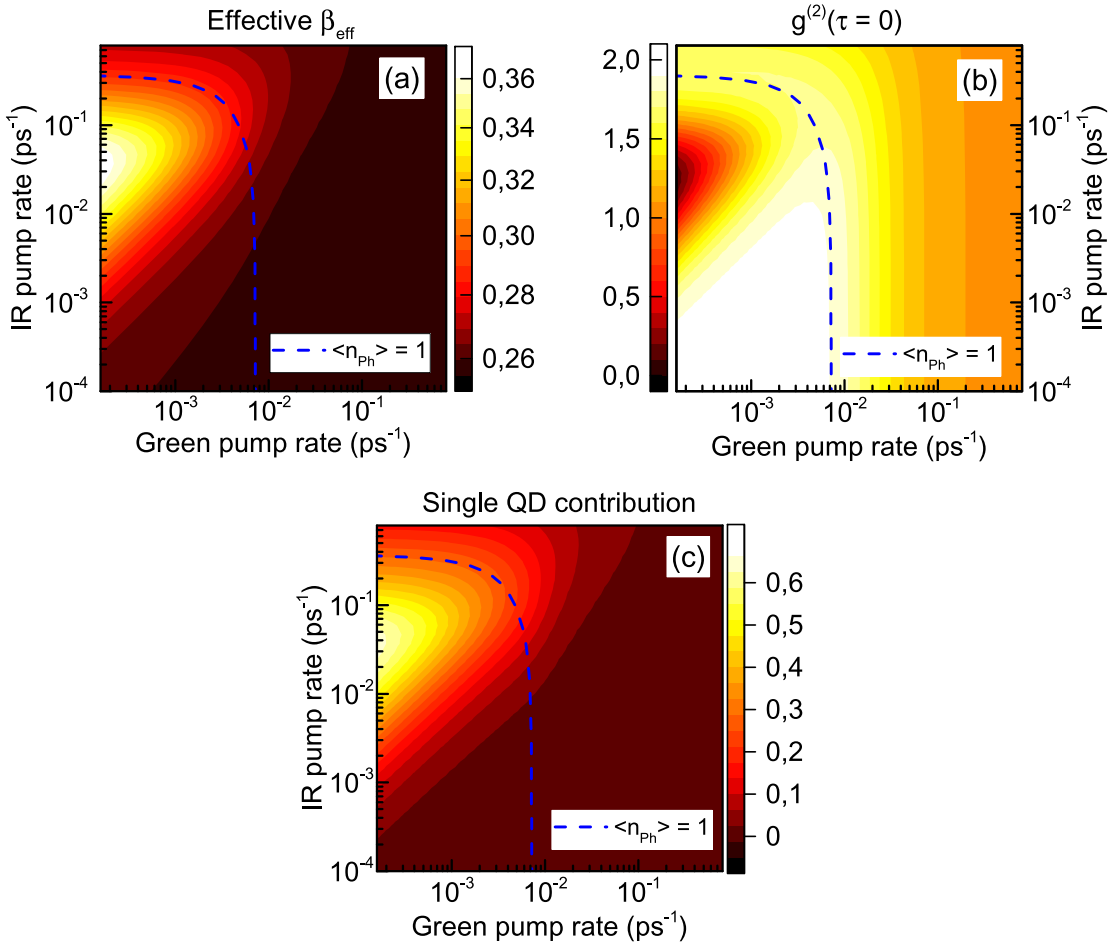

Figure 6. With the two-color pump rates on both axes, numerical results are shown for (a) the effective β-factor, (b) $g^{(2)}(\tau = 0)$, and (c) the contribution of the single target QD to the total micropillar output, which is evaluated as the relative difference between the total emission intensity of the full system, and the total emission of the BG emitters for parameters corresponding to the system investigated experimentally. In all graphs the laser threshold ($\langle n_{\mathrm{Ph}} \rangle = 1$) is marked by a blue dashed line.

which case the single-QD is removed in the modeling). This cannot be realized in our experiments, as the presence of the single-QD is noticeable even if is not directly excited. Thus, the theoretical analysis gives important insight beyond the experimentally accessible regime and is very informative as it separates the two contributions to the microlaser output (for details see appendix). Noteworthy, this analysis that goes well beyond the description of conventional semiconductor lasers in which the gain contribution of a single emitter is insignificant. It reveals contributions of up to 70% of the emission intensity due to a single resonant QD and unveils regions where the emission of a single-QD shows saturation (at high IR excitation pump rates exceeding 0.1 ps^{-1}). In their sum, the isolated contribution of the single-QD and the effective β-factor provide important insight into the interplay of resonant and background contributions in a nanolaser that can operate close to the ideal regime of single-emitter lasing. This insight could not be obtained from $g^{(2)}(\tau = 0)$ alone, which is a more intricate quantity as it reflects the properties of the photons in the cavity, rather than their origin. At the same time, the autocorrelation function obtained from our microscopic model demonstrates that a single device can be operated in any regime of non-classical, coherent, or thermal emission by choosing the resonant (IR) and background (green) excitation to realize any point in the two-color maps. Due to the high relevance of the photon statistics to understand the nature of the micropillar emission, it will be interesting to address the autocorrelation function under two-color excitation in future experimental studies in order to confirm the predictions of figure 6(b).

4. Conclusions

We have presented a comprehensive experimental and theoretical analysis of the relative gain contribution of a single resonant emitter and background emitters that are off-resonant in the single-QD lasing regime. Experimentally, this study is enabled by a two-color excitation scheme in a lateral excitation/axial detection

experimental configuration in which QDs can be excited directly at any wavelength. The contribution of the off-resonant QDs is controlled optically by above-band excitation, meanwhile the single-QD in resonance is excited selectively via its p-shell. This advanced excitation scheme allowed us to demonstrate and control a transition between a device with characteristics similar to those of a macroscopic laser with QD-ensemble gain, and a microlaser fed by a very limited and discrete gain which requires a quantum-optical description of the interaction between the QD emitters and photons in the cavity. Our study provides important insight into the operation of high-quality microlasers close to the limiting case of the thresholdless single-emitter laser. In particular, it allows us to distinguish between a single- and a multiple-QD laser, a task which cannot be done solely based on the input–output characteristics.

We reveal that a dominant single-QD gain contribution leads to a higher effective β-factor. This is a key aspect of our work, which shows that, in contrast the usual understanding, the β-factor is not constant for a given microcavity system, but depends on and can be controlled by the specific excitation conditions determining the effective gain. The dominant single-QD role is further evidenced in the photon statistics. Both, the lasing threshold and the effective β-factor, strongly depend on non-resonant gain contribution. Nevertheless, even if the efficiency of the spontaneous-emission coupling to the lasing mode is degraded by off-resonant emitters, lasing conditions can be reached in our system due to additional emitters.

The developed experimental approach is a very powerful technique enabling continuous change of the output characteristics of a single microlaser device using selective excitation of its gain. It constitutes an alternative to more complicated schemes, where precise or even deterministic control of the position, number, and optical characteristics of QDs in the active material during growth or processing is utilized. Our analysis demonstrates that the off-resonant QDs lower the threshold power and result in restoring a pronounced s-shape in the input–output curve, but simultaneously cause a drop in the effective β-factor of our QD-based micropillar laser. Therefore, the contribution of the non-resonant QDs can be used to control and tailor those two correlated laser parameters. As such our work provides important insight into the relative contribution of a resonant emitter and non-resonant BG emitters on the emission properties of a microlaser, which will be of high relevance for the further development of micro- and nanolasers towards the ultimate thresholdless single-quantum-dot laser.

Acknowledgments

The research leading to these results has received funding from the European Research Council under the European Union's Seventh Framework ERC Grant Agreement No. 615613 as well as from the German Research Foundation via Grant-No.: Re2974/10-1, Gi1121/1-1, and Ka 2318/7-1. We gratefully thank M Sommer for technical assistance.

Appendix A

In the main text figure 3(b), one would expect saturation behavior of the input–output curve under p-shell excitation of the target QD. However, saturation is not observed and that can be attributed to different reasons, e.g., due to insufficient excitation power or due to contribution of off-resonant emitters. Here, we describe experimental findings that clarify the reason why the expected saturation is not observed. For that, we study the limiting case of truly selective excitation of a target QD, i.e., strictly resonant s-shell excitation has been employed. In that case none of the BG (off-resonant) emitters is excited directly as the laser energy is tuned to match the QD X transition of the target QD strongly-coupled and in resonance with the cavity mode. Interestingly, a residual excitation redistribution via the cavity mode due to cavity-mediated coupling between the dots is still visible in the broad range spectrum (not-shown here). So that even under resonant s-shell excitation of the target QD the BG emitters light up, although their contribution to the emission is negligible in comparison to the target QD in resonance with the cavity mode. For this proof-of-principle experiment, a QD-micropillar (with vacuum Rabi splitting as large as 127 μeV) in the same investigated sample was chosen to enable extraction of the signal of the target QD coupled to the cavity mode even in the case of non-ideal laser suppression. The same tunable IR laser is also used for strictly resonant s-shell excitation, but in this case, additional measures have to be taken to suppress stray light excitation, i.e., polarization rejection of the resonant laser and spatial filtering of the detected signal using confocal configuration [53].

In the RF intensity map (figure A1(b)) as well as in the single low-excitation spectrum (figure A1(a)), a strong resonance at the QD X energy (marked with green dotted–dashed line) and two much weaker maxima are visible. These maxima, that are two orders of magnitude weaker than the main resonance, correspond to the Rabi doublet and are indicated by the dotted–dashed black line in both panels. The middle peak contains the contribution from the emission and laser scattered on the (uncoupled) QD X as well as undesired laser stray light. The corresponding input–output curve is presented in figure A1(c). The sum of integrated intensities of the Rabi doublet (evaluated after subtracting the fitted middle resonance) is depicted on the vertical axis. The QD

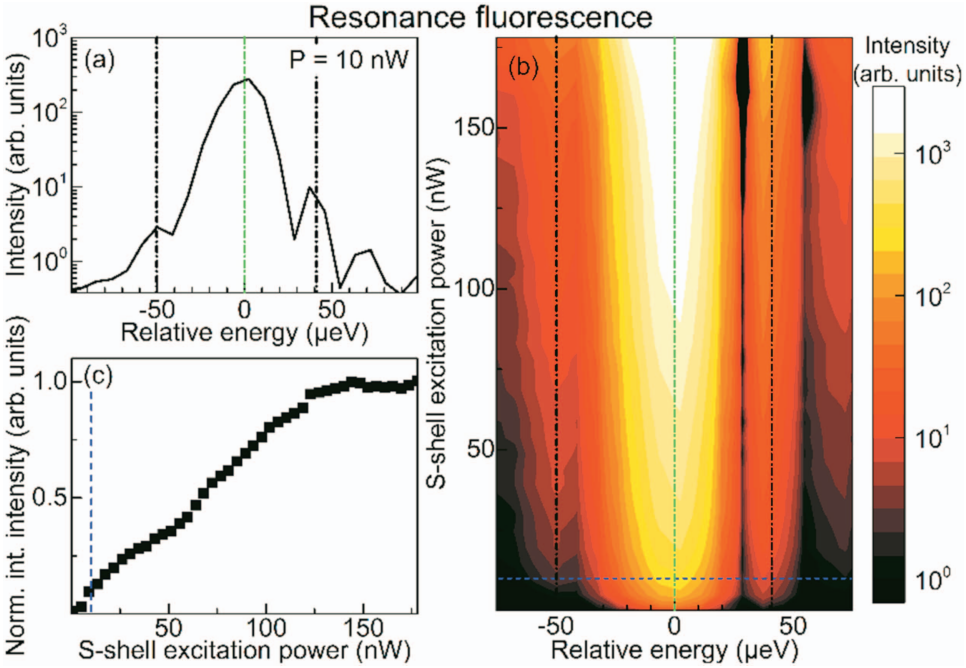

Figure A1. Strongly-coupled single QD exciton (X) and cavity photon under resonant (s-shell) excitation. All energies are relative with respect to the laser energy (indicated by green dotted–dashed vertical line in (a) and (b)) resonant with the bare (uncoupled) QD X transition. (a) Resonance fluorescence (RF) spectrum at intermediate excitation power of 10 nW. The Rabi doublet is marked with black dotted–dashed vertical lines; (b) 2D RF intensity map as a function of excitation power; (c) integrated RF intensity of the Rabi doublet as a function of excitation power. The s-shell excitation power of 10 nW (corresponding to spectrum in (a)) is indicated by a dashed black line in panels (b) and (c).

X transition shows saturation at an excitation power of around 150 nW, which is 2 orders of magnitude lower than typically for off-resonant excitation of the QDs. This clearly illustrates higher excitation efficiency of resonant driving. This proves that only a single QD is feeding the cavity as intended. However, this single QD does not provide enough gain to drive the system into lasing as shown also previously for similar system [10]. This has important consequences for the interpretation of figure 3(b) in the main text. Taking into account the different excitation efficiencies of various excitation schemes, the saturation of the single QD would still be expected in the range of excitation powers available for p-shell excitation. The fact that we do not observe its signatures in the input–output curve (see figure 3(b) in the main text) shows that indeed the off-resonant emitters are directly excited and can even dominate the output of the QD-micropillar at high excitation.

Appendix B

The present work draws on lasers with two distinct excitation wavelengths to address a selected resonant QD and the BG emitters and to investigate the influence of the latter on the former. The theoretical investigation is based on a modified version of the semiconductor laser model established in [52], while considering the two-color excitation scheme as realized in the experiment.

B.1. Laser equations

We start from a microscopic Hamiltonian for the QD electronic states, the quantized electromagnetic field, and the interaction of the QD excitonic transitions with photons in the cavity mode to obtain the coupled semiconductor laser equations for the carrier dynamics $f_\nu^{e,h}$, photons dynamics $\langle b^\dagger b\rangle$, and the dynamics of the photon assisted polarization $\langle b^\dagger v_\nu^\dagger c_\nu\rangle$, as well as higher-order correlation functions between electronic and photonic operators. For details, we refer to [52], where the laser equations are derived up to the level of the second-order photon autocorrelation function $g^{(2)}(0)$.

The experiment realizes the particular situation, where a single QD emitter is tuned into perfect resonance with the cavity mode, while a number N of additional emitters acts as a background that is detuned from the mode. In the laser equations, we distinguish these two components by an index ξ denoting the resonant dot

(QD) and the BG emitters. With this, the mean photon number is determined by

$$\hbar\frac{\mathrm{d}}{\mathrm{d}t}\langle b^\dagger b\rangle = -2\kappa\langle b^\dagger b\rangle + |g_{\mathrm{QD}}|^2\langle b^\dagger \nu_{\mathrm{QD}}^\dagger c_{\mathrm{QD}}\rangle + \sum_{\xi=\mathrm{BG}}|g_\xi|^2\langle b^\dagger \nu_\xi^\dagger c_\xi\rangle \tag{B.1}$$

and contains contributions from the photon-assisted polarization of both the resonant and detuned emitters (the second summation is over all BG emitters). Cavity losses are included as the rate 2κ.

The photon-assisted polarization is the central quantity of the laser model, as it contains the physical processes of spontaneous and stimulated emission caused by the light–matter interaction. As the parameters differ for the two different subsystems, it also depends on ξ:

$$\hbar\frac{\mathrm{d}}{\mathrm{d}t}\langle b^\dagger \nu^\dagger c\rangle_\xi = -(\kappa+\Gamma_\xi)\langle b^\dagger \nu^\dagger c\rangle_\xi + f_{s,\xi}^e f_{s,\xi}^h + (1 - f_{s,\xi}^e - f_{s,\xi}^h)\langle b^\dagger b\rangle, \quad \xi\in\{\mathrm{QD},\,\mathrm{BG}\}. \tag{B.2}$$

In this equation, Γ is a phenomenological broadening of the QD transition, the term proportional to the QD s-shell electron and hole population results in the spontaneous emission contribution, while stimulated emission or absorption is proportional to the mean intra-cavity photon number and the inversion of each emitter.

The QD carrier population of the lowest energy s-states is determined by the interplay of recombination into the laser mode via the photon-assisted polarization, radiative losses into non-lasing modes $R_{\mathrm{nl}} = (1-\beta)f_\nu^e f_\nu^h/\tau_{\mathrm{sp}}$, and in-scattering of carriers from the energetically higher QD p-states at rates $R_{p\to\nu}^{e,h}$:

$$\hbar\frac{\mathrm{d}}{\mathrm{d}t}f_{s,\mathrm{QD}}^{e,h} = -2\,|g_{\mathrm{QD}}|^2\langle b^\dagger \nu^\dagger c\rangle_{\mathrm{QD}} + R_{\mathrm{nl}}(\beta_{\mathrm{QD}}) + R_{p\to s}^{e,h}(P_{\mathrm{IR}}), \tag{B.3}$$

$$\hbar\frac{\mathrm{d}}{\mathrm{d}t}f_{s,\mathrm{BG}}^{e,h} = -2\,|g_{\mathrm{BG}}|^2\langle b^\dagger \nu^\dagger c\rangle_{\mathrm{BG}} + R_{\mathrm{nl}}(\beta_{\mathrm{BG}}) + R_{p\to s}^{e,h}(P_{\mathrm{IR}}, P_{\mathrm{BG}}). \tag{B.4}$$

Non-resonant carrier excitation is modeled by carrier generation into the higher QD p-states, either via direct excitation in case of IR excitation at rate P_{IR}, or via in-scattering of carriers that are excited into the energetically higher-lying states of the barrier material by green laser excitation at rate P_{G}:

$$\hbar\frac{\mathrm{d}}{\mathrm{d}t}f_{p,\mathrm{BG}}^{e,h} = (P_{\mathrm{G}} + \eta P_{\mathrm{IR}})(1 - f_{p,\mathrm{BG}}^e - f_{p,\mathrm{BG}}^h) - R_{p\to s}^{e,h}(P_{\mathrm{IR}}), \tag{B.5}$$

$$\hbar\frac{\mathrm{d}}{\mathrm{d}t}f_{p,\mathrm{QD}}^{e,h} = P_{\mathrm{IR}}(1 - f_{p,\mathrm{QD}}^e - f_{p,\mathrm{QD}}^h) - R_{p\to s}^{e,h}(P_{\mathrm{IR}}, P_{\mathrm{BG}}). \tag{B.6}$$

The dependence of the rate $R_{p\to\nu}^{e,h}$ on both P_{IR} and P_{G} is motivated by the experimental fact that a small fraction of the the IR laser is also captured by the BG emitters.

To access the second-order correlation function given by

$$g^{(2)}(0) = 2 + \frac{\delta\langle b^\dagger b^\dagger b b\rangle}{\langle b^\dagger b\rangle^2}, \tag{B.7}$$

we consider for each subsystem expectation values containing up to four photon operators in the arising hierarchy, while higher-order correlation functions are truncated [52]. However, as above, the higher-order correlation function must be modified with respect to the equation given in [52] to account for the two-excitation-scheme:

$$\hbar\frac{\mathrm{d}}{\mathrm{d}t}\delta\langle b^\dagger b^\dagger b b\rangle = -4\kappa\delta\langle b^\dagger b^\dagger b b\rangle + 4\sum_{\xi=\mathrm{QD}}|g_\xi|^2\langle b^\dagger b^\dagger b \nu_\xi^\dagger c_\xi\rangle + 4\sum_{\xi=\mathrm{BG}}|g_\xi|^2\langle b^\dagger b^\dagger b \nu_\xi^\dagger c_\xi\rangle. \tag{B.8}$$

B.2. Choice of parameters

As described in the context of figure 3 in the main text, the parameters of the two subsystems (BG emitters and single resonant QD) are based on a comparison between theory and experiment using green and IR excitation separately. This comparison is done by matching the calculated input–output characteristics to the measured one. The β factors of the resonant QD ($\beta_{\mathrm{QD}} = 0.9$) and the background ($\beta_{\mathrm{BG}} = 0.25$) are determined by the matching the height of the jump between experimental and theoretical results.

An estimate for the light–matter coupling constant of $g_{\mathrm{QD}} = 50\ \mu$eV for the resonant QD is known from experimental measurements and provides an upper bound for the coupling constant of the BG emitters, for which we use $g_{\mathrm{BG}} = 20\ \mu$eV. A Q-factor of 15 000 has been determined experimentally for the laser mode. Typical values are used for the relaxation rates (1 ps and 2 ps for electrons and holes, respectively) and the dephasing rates ($\Gamma_{\mathrm{QD}} = 1.36\ \mu$eV and $\Gamma_{\mathrm{BG}} = 80\ \mu$eV). We have checked that small variations of the dephasing rates result in qualitatively the same behavior. $N = 160$ BG emitters have been used. These parameters have been used for all calculations throughout the manuscript.

The BG emitters are distributed over a spectral range of tens of meV. In principle, depending on the individual detuning situation, cavity-feeding rates differ for all emitters, especially due to the differences in the efficiency of the underlying off-resonant coupling mechanisms. Since the exact spectral positions are not known

and in order to avoid microscopic calculations of phonon- or Auger-assisted feeding rates [27, 34, 54], we consider their contribution as an ensemble average. An effective light–matter coupling and β factor is determined that apply equally for all BG emitters in the model.

B.3. Derivation of the effective spontaneous emission factor

In the main text we provide an analytical formula for the effective spontaneous emission factor of the joint system of resonant dot and the BG emitters that couples to the same photonic mode. Per definition, the spontaneous emission factor is the fraction of the total spontaneous emission that is funneled into the cavity mode, i.e.

$$\beta = \frac{\gamma_{\mathrm{l}}}{\gamma_{\mathrm{l}} + \gamma_{\mathrm{nl}}}, \tag{B.9}$$

where γ_{l} and γ_{nl} are the rate of spontaneous emission into the lasing and nonlasing modes, respectively. From the semiconductor laser model with the two-color excitation scheme, we define an effective β factor as

$$\begin{aligned}\beta_{\mathrm{eff}} &= \frac{\gamma_{\mathrm{l}}^{\mathrm{QD}} + \gamma_{\mathrm{l}}^{\mathrm{BG}}}{\gamma_{\mathrm{l}}^{\mathrm{QD}} + \gamma_{\mathrm{nl}}^{\mathrm{QD}} + \gamma_{\mathrm{l}}^{\mathrm{BG}} + \gamma_{\mathrm{nl}}^{\mathrm{BG}}} \\ &= \frac{\gamma_{\mathrm{l}}^{\mathrm{QD}}}{\gamma_{\mathrm{l}}^{\mathrm{QD}} + \gamma_{\mathrm{nl}}^{\mathrm{QD}} + \gamma_{\mathrm{l}}^{\mathrm{BG}} + \gamma_{\mathrm{nl}}^{\mathrm{BG}}} + \frac{\gamma_{\mathrm{l}}^{\mathrm{BG}}}{\gamma_{\mathrm{l}}^{\mathrm{QD}} + \gamma_{\mathrm{nl}}^{\mathrm{QD}} + \gamma_{\mathrm{l}}^{\mathrm{BG}} + \gamma_{\mathrm{nl}}^{\mathrm{BG}}}.\end{aligned} \tag{B.10}$$

In the steady state, the spontaneous emission rate from each subsystem is given by

$$\gamma_{\mathrm{l}}^{\xi} = 2N_{\xi} g_{\xi}^{2} \langle b^{\dagger} \nu^{\dagger} c \rangle_{\xi} \tag{B.11}$$

and depends on the photon-assisted polarization, the value of which can be obtained by solving its corresponding equation of motion in the steady state

$$0 = -(\kappa_{\xi} + \Gamma_{\xi}) \langle b^{\dagger} \nu^{\dagger} c \rangle_{\xi} + f_{\xi}^{\mathrm{e}} f_{\xi}^{\mathrm{h}}. \tag{B.12}$$

Note that we have omitted the stimulated emission channel, as only photons stemming from spontaneous emission enter the definition and computation of the β factor. The loss into the nonlasing modes can be read from the population dynamics in the s-shell and is given by

$$\gamma_{\mathrm{nl}}^{\xi} = N_{\xi}(1 - \beta_{\xi}) \frac{f_{\xi}^{e} f_{\xi}^{h}}{\tau_{\mathrm{sp}}^{\xi}}. \tag{B.13}$$

By combining the above equations and using the definition of the light–matter coupling in terms of the spontaneous emission time [52]

$$g_{\xi}^{2} = \frac{\hbar \beta_{\xi} (\kappa_{\xi} + \Gamma_{\xi})}{2\tau_{\mathrm{sp}}^{\xi}}, \tag{B.14}$$

we obtain the expression used in the main text for the effective β-factor

$$\beta_{\mathrm{eff}} = \frac{\beta_{\mathrm{QD}}}{1 + \frac{N}{\lambda} \frac{\langle b^{\dagger} \nu^{\dagger} c \rangle_{\mathrm{BG}}}{\langle b^{\dagger} \nu^{\dagger} c \rangle_{\mathrm{QD}}}} + \frac{\beta_{\mathrm{BG}}}{1 + \frac{\lambda}{N} \frac{\langle b^{\dagger} \nu^{\dagger} c \rangle_{\mathrm{QD}}}{\langle b^{\dagger} \nu^{\dagger} c \rangle_{\mathrm{BG}}}}, \quad \lambda = \frac{\beta_{\mathrm{BG}}}{\beta_{\mathrm{QD}}} \left| \frac{g_{\mathrm{QD}}}{g_{\mathrm{BG}}} \right|^{2}. \tag{B.15}$$

References

[1] Noda S 2006 Seeking the ultimate nanolaser *Science* **314** 260–1
[2] Xie Z, Götzinger S, Fang W, Cao H and Solomon G 2007 Influence of a single quantum dot state on the characteristics of a microdisk laser *Phys. Rev. Lett.* **98** 117401
[3] Reitzenstein S *et al* 2008 Single quantum dot controlled lasing effects in high-Q micropillar cavities *Opt. Express* **16** 4848–57
[4] Nomura M, Kumagai N, Iwamoto S, Ota Y and Arakawa Y 2009 Photonic crystal nanocavity laser with a single quantum dot gain *Opt. Express* **17** 15975
[5] Nomura M, Kumagai N, Iwamoto S, Ota Y and Arakawa Y 2010 Laser oscillation in a strongly coupled single-quantum-dot-nanocavity system *Nat. Phys.* **6** 279–83
[6] Arakawa Y, Iwamoto S, Nomura M, Tandaechanurat A and Ota Y 2012 Cavity quantum electrodynamics and lasing oscillation in single quantum dot-photonic crystal nanocavity coupled systems *IEEE J. Sel. Top. Quantum Electron.* **13** 1818–29
[7] Strauf S and Jahnke F 2011 Single quantum dot nanolaser *Laser Photonics Rev.* **5** 607–33
[8] Birkedal D, Leosson K and Hvam J M 2001 Long lived coherence in self-assembled quantum dots *Phys. Rev. Lett.* **87** 227401
[9] Liu J, Ates S, Lorke M, Mørk J, Lodahl P and Stobbe S 2013 A comparison between experiment and theory on few-quantum-dot nanolasing in a photonic-crystal cavity *Opt. Express* **21** 28507
[10] Gies C *et al* 2017 Strong light–matter coupling in the presence of lasing *Phys. Rev.* A **96** 023806
[11] Pelucchi E *et al* 2007 Mechanisms of quantum dot energy engineering by metalorganic vapor phase epitaxy on patterned nonplanar substrates *Nano Lett.* **7** 1282

[12] Surrente A, Gallo P, Felici M, Dwir B, Rudra A and Kapon E 2009 Dense arrays of ordered pyramidal quantum dots with narrow linewidth photoluminescence spectra *Nanotechnology* **20** 415205
[13] Pfau T J, Gushterov A, Reithmaier J P, Cestier I, Eisenstein G, Linder E and Gershoni D 2013 Phonon-mediated off-resonant coupling effects in semiconductor quantum-dot lasers *New J. Phys.* **15** 035019
[14] Schneider C *et al* 2012 Single site-controlled In(Ga)As/GaAs quantum dots: growth, properties and device integration *Nanotechnology* **20** 434012
[15] Strittmatter A *et al* 2012 Lateral positioning of InGaAs quantum dots using a buried stressor *Appl. Phys. Lett.* **100** 093111
[16] Lee K H *et al* 2006 Registration of single quantum dots using cryogenic laser photolithography *Appl. Phys. Lett.* **88** 193106
[17] Dousse A *et al* 2008 Controlled light–matter coupling for a single quantum dot embedded in a pillar microcavity using far-field optical lithography *Phys. Rev. Lett.* **101** 267404
[18] Gschrey M *et al* 2013 *In situ* electron-beam lithography of deterministic single-quantum-dot mesa-structures using low-temperature cathodoluminescence spectroscopy *Appl. Phys. Lett.* **102** 251113
[19] He Y M *et al* 2017 Deterministic implementation of a bright, on-demand single photon source with near-unity indistinguishability via quantum dot imaging *Optica* **4** 802–8
[20] Sapienza L, Davanço M, Badolato A and Srinivasan K 2015 Nanoscale optical positioning of single quantum dots for bright and pure single-photon emission *Nat. Commun.* **6** 7833
[21] Gies C, Florian M, Gartner P and Jahnke F 2011 The single quantum dot-laser: lasing and strong coupling in the high-excitation regime *Opt. Express* **19** 14370
[22] Reithmaier J P, Sęk G, Löffler A, Hofmann C and Kuhn S 2004 Strong coupling in a single quantum dot-semiconductor microcavity system *Nature* **432** 197–200
[23] Hennessy K *et al* 2007 Quantum nature of a strongly coupled single quantum dot–cavity system *Nature* **445** 896–9
[24] Press D *et al* 2007 Photon antibunching from a single quantum-dot-microcavity system in the strong coupling regime *Phys. Rev. Lett.* **98** 117402
[25] Roy C and Hughes S 2011 Influence of electron-acoustic-phonon scattering on intensity power broadening in a coherently driven quantum-dot–cavity system *Phys. Rev.* X **1** 021009
[26] Winger M *et al* 2009 Explanation of photon correlations in the far-off-resonance optical emission from a quantum-dot-cavity system *Phys. Rev. Lett.* **103** 207403
[27] Florian M, Gartner P, Steinhoff A, Gies C and Jahnke F 2014 Coulomb-assisted cavity feeding in nonresonant optical emission from a quantum dot *Phys. Rev.* B **89** 161302
[28] Laucht A, Kaniber M, Mohtashami A, Hauke N, Bichler M and Finley J J 2010 Temporal monitoring of nonresonant feeding of semiconductor nanocavity modes by quantum dot multiexciton transitions *Phys. Rev.* B **81** 241302
[29] Blood P 2013 The laser diode: 50 years on *IEEE J. Sel. Top. Quantum Electron.* **19** 1503201
[30] Coldren L 2013 What is a diode laser oscillator? *IEEE J. Sel. Top. Quantum Electron.* **19** 1503503
[31] Ning C Z 2013 What is laser threshold? *IEEE J. Sel. Top. Quantum Electron.* **19** 1503604
[32] Chow W W, Jahnke F and Gies C 2014 Emission properties of nanolasers during the transition to lasing *Light: Sci. Appl.* **3** e201
[33] Kreinberg S *et al* 2017 Emission from quantum-dot high-β microcavities: transition from spontaneous emission to lasing and the effects of superradiant emitter coupling *Light: Sci. Appl.* **6** e17030
[34] Settnes M, Kaer P, Moelbjerg A and Mørk J 2013 Auger processes mediating the nonresonant optical emission from a semiconductor quantum dot embedded inside an optical cavity *Phys. Rev. Lett.* **111** 067403
[35] Choi Y S *et al* 2007 Evolution of the onset of coherence in a family of photonic crystal nanolasers *Appl. Phys. Lett.* **91** 031108
[36] Yokoyama H 1992 Physics and device applications of optical microcavities *Science* **256** 66–70
[37] Assmann M, Veit F, Bayer M, van der Poel M and Hvam J M 2009 Higher-order photon bunching in a semiconductor microcavity *Science* **325** 297–300
[38] Nomura M, Iwamoto S, Kumagai N and Arakawa Y 2007 Temporal coherence of a photonic crystal nanocavity laser with high spontaneous emission coupling factor *Phys. Rev.* B **75** 195313
[39] Hostein R *et al* 2010 Demonstration of coherent emission from high-β photonic crystal nanolasers at room temperature *Opt. Lett.* **35** 1154
[40] Hachair X *et al* 2011 Identification of the stimulated-emission threshold in high-β nanoscale lasers through phase-space reconstruction *Phys. Rev.* A **83** 053836
[41] Lu Y J *et al* 2012 Plasmonic nanolaser using epitaxially grown silver film *Science* **337** 450–3
[42] Gregersen N, Suhr T, Lorke M and Mørk J 2012 Quantum-dot nano-cavity lasers with Purcell-enhanced stimulated emission *Appl. Phys. Lett.* **100** 131107
[43] Lichtmannecker S *et al* 2017 A few-emitter solid-state multi-exciton laser *Sci. Rep.* **7** 7420
[44] Ates S, Ulrich S M, Reitzenstein S, Löffler A, Forchel A and Michler P 2009 Post-selected indistinguishable photons from the resonance fluorescence of a single quantum dot in a microcavity *Phys. Rev. Lett.* **103** 167402
[45] Reitzenstein S *et al* 2007 AlAs/GaAs micropillar cavities with quality factors exceeding 150.000 *Appl. Phys. Lett.* **90** 251109
[46] Musiał A *et al* 2015 Correlations between axial and lateral emission of coupled quantum dot-micropillar cavities *Phys. Rev.* B **91** 205310
[47] Cusack M A, Briddon P R and Jaros M 1996 Electronic structure of InAs/GaAs self-assembled quantum dots *Phys. Rev.* B **54** R2300–3
[48] Brounkov P N, Polimeni A, Stoddart S T, Henini M and Eaves L 1998 Electronic structure of self-assembled InAs quantum dots in GaAs matrix *Appl. Phys. Lett.* **73** 1092–4
[49] Narvaez A, Bester G and Zunger A 2005 Dependence of the electronic structure of self-assembled (In,Ga)As/GaAs quantum dots on height and composition *J. Appl. Phys.* **98** 043708
[50] Hopfmann C *et al* 2016 Effcient stray-light suppression for resonance fluorescence in quantum dot micropillars using self-aligned metal apertures *Semicond. Sci. Technol.* **31** 095007
[51] Musiał A *et al* 2014 Toward weak confinement regime in epitaxial nanostructures: Interdependence of spatial character of quantum confinement and wave function extension in large and elongated quantum dots *Phys. Rev.* B **90** 045430
[52] Gies C, Wiersig J, Lorke M and Jahnke F 2007 Semiconductor model for quantum-dot based microcavity lasers *Phys. Rev.* A **75** 013803
[53] Hopfmann C *et al* 2017 Transition from Jaynes–Cummings to Autler-Townes ladder in a quantum dot-microcavity system *Phys. Rev.* B **95** 035302
[54] Florian M, Gartner P, Gies C and Jahnke F 2013 Phonon-mediated off-resonant coupling effects in semiconductor quantum-dot lasers *New J. Phys.* **15** 035019
[55] Capua A, Karni O, Eisenstein G, Reithmaier J P and Yvind K 2012 Extreme nonlinearities in InAs/InP nanowire gain media: the two-photon induced laser *Opt. Express* **20** 5987